Detection of Macular Ganglion Cell Loss in Glaucoma by Fourier-Domain Optical Coherence Tomography

Ou Tan, PhD,[1] Vikas Chopra, MD,[1] Ake Tzu-Hui Lu, PhD,[1] Joel S. Schuman, MD,[2] Hiroshi Ishikawa, MD,[2] Gadi Wollstein, MD,[2] Rohit Varma, MD, MPH,[1] David Huang, MD, PhD[1]

Purpose: To map ganglion cell complex (GCC) thickness with high-speed Fourier-domain optical coherence tomography (FD-OCT) and compute novel macular parameters for glaucoma diagnosis.

Design: Observational, cross-sectional study.

Participants: One hundred seventy-eight participants in the Advanced Imaging for Glaucoma Study, divided into 3 groups: 65 persons in the normal group, 78 in the perimetric glaucoma group (PG), and 52 in the preperimetric glaucoma group (PPG).

Methods: The RTVue FD-OCT system was used to map the macula over a 7×6 mm region. The macular OCT images were exported for automatic segmentation using software we developed. The program measured macular retinal (MR) thickness and GCC thickness. The GCC was defined as the combination of nerve fiber, ganglion cell, and inner plexiform layers. Pattern analysis was applied to the GCC map and the diagnostic powers of pattern-based diagnostic parameters were investigated. Results were compared with time-domain (TD) Stratus OCT measurements of MR and circumpapillary nerve fiber layer (NFL) thickness.

Main Outcome Measures: Repeatability was assessed by intraclass correlation, pooled standard deviation, and coefficient of variation. Diagnostic power was assessed by the area under the receiver operator characteristic (AROC) curve. Measurements in the PG group were the primary measures of performance.

Results: The FD-OCT measurements of MR and GCC averages had significantly better repeatability than TD-OCT measurements of MR and NFL averages. The FD-OCT GCC average had significantly ($P = 0.02$) higher diagnostic power (AROC = 0.90) than MR (AROC = 0.85 for both FD-OCT and TD-OCT) in differentiating between PG and normal. One GCC pattern parameter, global loss volume, had significantly higher AROC (0.92) than the overall average ($P = 0.01$). The diagnostic powers of the best GCC parameters were statistically equal to TD-OCT NFL average.

Conclusions: The higher speed and resolution of FD-OCT improved the repeatability of macular imaging compared with standard TD-OCT. Ganglion cell mapping and pattern analysis improved diagnostic power. The improved diagnostic power of macular GCC imaging is on par with, and complementary to, peripapillary NFL imaging. Macular imaging with FD-OCT is a useful method for glaucoma diagnosis and has potential for tracking glaucoma progression.

Financial Disclosure(s): Proprietary or commercial disclosure may be found after the references.
Ophthalmology 2009;116:2305–2314

Glaucoma is characterized by loss of retinal ganglion cells (RGCs) and their respective axons, which comprise the retinal nerve fiber layer (RNFL), on pathologic examination.[1–5] RGC loss cannot be seen on slit-lamp ophthalmic examination. Likewise, nerve fiber layer (NFL) bundle defects are difficult to detect on clinical examination, and red-free fundus photography to identify and characterize them is rarely used in clinical practice. Thus, glaucoma is diagnosed based on characteristic optic nerve cupping with corresponding visual field (VF) deficits. However, because a significant loss to RGC population can occur before detectable VF deficits and that structural loss can precede detectable function loss by up to 5 years,[6–9] developing methods to quantify RGC-related glaucomatous changes could lead to glaucoma detection at an earlier stage and more accurate tracking of glaucoma progression.

A significant proportion of RGC population resides in the macula, but is clinically undetectable on ophthalmoscopic examination. Reduced macular thickness in glaucoma was initially described by Zeimer et al[10] using the slit-scanning Retinal Thickness Analyzer (Talia Technology Ltd., Neve-Ilan, Israel). Since the introduction of optical coherence tomography (OCT) by Huang et al,[11] it has proven useful for measuring circumpapillary NFL thickness for glaucoma detection. However, total macular retinal (MR) thickness measurement using OCT has

ISSN 0161-6420/09/$–see front matter
doi:10.1016/j.ophtha.2009.05.025

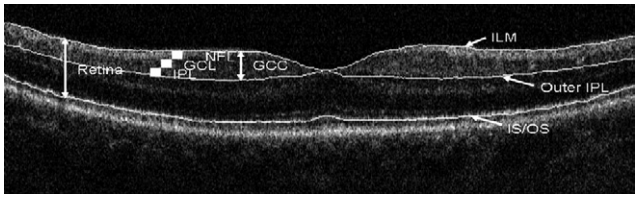

Figure 1. Vertical optical coherence tomography (OCT) cross-section of the macula. The image was acquired using the RTVue Fourier-domain (FD)-OCT system. The ganglion cell complex (GCC) consists of 3 layers: the nerve fiber layer (NFL), ganglion cell layer (GCL), and inner plexiform layer (IPL). The 3 boundaries on the image are inner limiting membrane (ILM), outer IPL boundary and inner segment/outer segment (IS/OS) junction. The GCC thickness is measured from the ILM to the outer IPL boundary. The retinal thickness is measured from the ILM to the IS/OS junction.

not been nearly as accurate a diagnostic parameter as NFL.[12–14]

Two recent studies from our group found that glaucoma diagnostic accuracy could be improved if macular measurements by OCT are focused on the inner retinal layers.[15,16] Glaucoma preferentially affects the 3 innermost retinal layers: the nerve fiber, ganglion cell, and inner plexiform layers, which contain, respectively, the axons, cell bodies, and dendrites of the ganglion cells. Therefore, we refer to the combination of these 3 layers as the ganglion cell complex (GCC; Fig 1).

In this study, we investigate the diagnostic potential of macular GCC thickness mapping and analysis using a newer Fourier-domain (FD)-OCT[17–20] system (also called spectral or spectral domain OCT[21–27]). The FD-OCT system has higher resolution and speed compared with the time-domain (TD) OCT system we previously studied. The higher speed enables mapping of the macula over a wider area with many more sampling points. The higher resolution facilitates delineation of GCC from the rest of retina. The potential for improved repeatability and diagnostic power was assessed in a cross-sectional clinical study.

Methods

Clinical Study

Participants in the prospective, longitudinal Advanced Imaging for Glaucoma Study (AIGS) between 2003 and 2007 were included. The earliest available FD-OCT scans for each participant, along with the TD-OCT taken at the same visit, were used in the analysis. Participants in the following 3 groups were analyzed: normal, perimetric glaucoma (PG), and preperimetric glaucoma (PPG). The eligibility criteria for the 3 groups analyzed are briefly described below, but were also described in our previous publication.[16] Further description of the AIG Study protocol can be found in the AIGS Manual of Procedures (http://www.aigstudy.net/index.php?id=12; accessed March 18, 2009).

The normal group participants had intraocular pressure of <21 mmHg for both eyes, a normal Humphrey SITA 24-2 standard VF (mean deviation [MD] and pattern standard deviation within 95% limits of the normal reference and a glaucoma hemifield test within 97% limits), a central corneal thickness ≥ 500 μm, a normal-appearing optic nerve head, a normal NFL, an open anterior chamber angle by gonioscopy, and no history of chronic ocular or systemic corticosteroid use.

The PG group participants had ≥ 1 eye that fulfilled the following criteria: glaucomatous (abnormal) VF loss (pattern standard deviation [$P<0.05$] or glaucoma hemifield test [$P<1\%$] outside normal limits in a consistent pattern on both qualifying VFs) and optic nerve head changes such as diffuse or localized rim thinning, disc (splinter) hemorrhage, vertical cup-to-disc ratio greater than the fellow eye by >0.2, or notch in the rim detected on baseline dilated fundus examination and confirmed by masked reading of stereo disc photographs.

The PPG group participants had same criteria for optic nerve head change as defined for the PG group, but did not have the VF loss criteria need to meet eligibility for the PG group.

Exclusion criteria for all groups in the AIGS are best-corrected visual acuity $<20/40$; age <40 or >79 years; spherical equivalent refractive error $>+3.00$ or <-7.00 diopters; diabetic retinopathy or other diseases that could cause VF loss or optic disc abnormalities; or previous intraocular surgery other than an uncomplicated cataract extraction with posterior chamber intraocular lens implantation.

The research was conducted in accordance with the Declaration of Helsinki. Informed consent was obtained from all participants after the goals of the study and consequences of participation had been discussed. The institutional review board of each institution involved in the study approved the research protocol.

Fourier-Domain Optical Coherence Tomography

Study participants were scanned using the RTVue FD-OCT system (Optovue, Inc., Fremont, CA), which acquires 26,000 axial scans (a-scans) per second and has a 5-μm depth resolution (full width, half maximum) in tissue. With the FD-OCT, we devised 3-dimensional scans of the macular region called the GCC scan that samples the macula with 14 928 a-scans over a 7-mm square area in 0.6 seconds (Fig 2). We chose to limit the scan time to 0.6 second to reduce the problems of eye movement and corneal drying associated with long scan time. The scan pattern consists of 1 horizontal line and 15 vertical lines at 0.5-mm intervals. The center of the GCC scan is shifted 0.75 mm temporally to improve sampling of the temporal periphery.

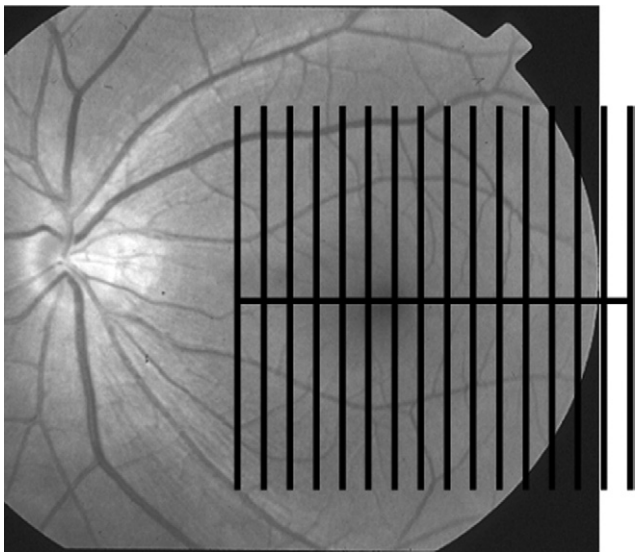

Figure 2. The ganglion cell complex scan pattern consists of 15 vertical and 1 horizontal scan lines shown overlaid on a red-free fundus photograph.

Image Acquisition

All participants were scanned 3 times with the GCC scan (formerly called MM7 scan on software versions 3.0 and earlier). RTVue software versions 1.0 to V3.0 were used for acquisition. The photographers rejected scans with motion artifacts (discontinuous jump). The photographers did not look for signal strength (SS) or segmentation error because the processing software was not available at the time the study started. The OCT images were exported using the XML export function of RTVue version 3.0 software. The exported image set included 16 B-scans (cross-sectional images), each with 640X933 (depth×width) pixels and 3×7.5 micron pixel size. The entire set contains 9 553 920 pixels.

Participants were also scanned with the Stratus TD-OCT system (Carl Zeiss Meditec, Dublin, CA), which acquires 400 a-scans per second and has a 10-μm resolution. Stratus OCT imaging was performed by the same photographer at the same visit using the fast RNFL scan and the fast macular thickness map scan. The RNFL scan consists of three 3.4-mm circles around the optic disc. The fast macular thickness map scan contains six 6-mm radial scans. Both patterns contain 768 a-scans completed in 2 seconds. Two sets of both scans were taken in each eye. According to the AIGS protocol, the photographer rejected scans with motion artifacts, segmentation error (>15% consecutive or >20% cumulative number of A-scans with wrong boundary by visual inspection) or SS <5 during the imaging session and took more scans to satisfy the criteria. For the purpose of this article, images with SS <6 were further excluded. Using the standard Stratus 4.0 software, the overall averages of circumpapillary NFL thickness and MR thicknesses were calculated.

Glaucoma severity was staged by MD and pattern standard deviation according to the Glaucoma Staging System 2.[28]

Image Processing

We developed automated software to map GCC. First, the 15 vertical OCT cross-section images (Fig 3A; available online at http://aaojournal.org) were aligned in the *z*-dimension (depth axis) to the horizontal image by cross correlation to build a registered 3-dimensional (3D) image set. To suppress background and speckle noises, each image was smoothed with a median filter.

To improve the speed and robustness of boundary detection, a progressive refinement procedure was applied. The procedure starts with boundary detection on a low-resolution (highly low-pass filtered) 3D data set and then progressively refines the boundary on progressively higher resolution (less filtered) data. A 2-dimensinoal version of this procedure was described in our previous work[16] and extended to 3D in the current algorithm.

The boundary detection algorithm starts with the photoreceptor pigment epithelium complex (PPC) band, which includes the bright bands of the photoreceptor inner segment-outer segment (IS/OS) junction and the retinal pigment epithelium. The PPC was detected as the second (counting from the inner side) maximum intensity peak in a low-resolution image (Fig 3B; available online at http://aaojournal.org). The IS/OS junction was then detected as the first maximum intensity peak within the PPC in the original resolution. Small portions of the PPC had low signal owing to shadowing from overlying blood vessels; these shadowed a-scans were replaced by adjacent a-scans to avoid interruption of boundary detection. The images were aligned at the IS/OS junction to facilitate lateral smoothing. The gradient image was then obtained by applied gradient operator to smoothed intensity image in depth direction.

The inner limiting membrane (ILM) was identified as the first positive gradient peak of each a-scan. Neighbor constraint and a knowledge model were used to distinguish the ILM peak from spurious noise or detached vitreous face. The outer plexiform layer (OPL) were detected as the first intensity peak above (inner to) the IS/OS. Then the outer boundary of the inner plexiform layer was identified as the negative gradient peak above the OPL peak (Fig 3C; available online at http://aaojournal.org). The accuracy of the segmentation was visually confirmed by one author (OT) on every B-scan. If the segmentation of ILM, OPL, or IS/OS boundary was off by >5 pixels in more than 1/6 of any B-scan, the GCC scan was excluded. Based on the experience from visual inspection, we decided to reject images with SS index (SSI) <38 because segmentation errors were too common below the SSI threshold.

The GCC thickness was measured from the ILM to the outer inner plexiform layer boundary. Retinal thickness was measured from the ILM to the IS/OS junction. The GCC (Fig 3D; available online at http://aaojournal.org) and MR maps were computed by interpolation of the thickness profiles from the 15 vertical B-scans in the 3D dataset. The interpolated map contains 933×933 points, which was interpolated from 933 a-scans×15 B-scans (each B-scan contained 933 a-scans). The interpolation used cubic spline interpolation function in MATLAB. Finally, the position of the foveal depression was identified on the MR map and used to recenter the vertical position of the maps. The fovea center was identified as the location of minimal retinal thickness on the low-pass filtered map within 0.5 mm of fixation. The maps were cropped to remove peripheral areas where segmentation was less reliable. The remaining areas are those within a 7-mm diameter circle and within 3 mm from the central horizontal line. For the GCC map (Fig 3E; available online at http://aaojournal.org), the area within 0.75 mm of the foveal center (1.5-mm diameter circle) was also excluded because the GCC is too thin to be reliably measured in that region. The GCC maps of all eyes in the normal group were averaged, point by point, to obtain the normal reference GCC map (Fig 3F; available online at http://aaojournal.org). The reference map is important for the calculation of GCC loss maps and pattern-based diagnostic parameters. The reference GCC map had a root-mean-square SD of 10 μm and standard error of 0.9 μm.

Derivation of Diagnostic Parameters

We computed several glaucoma diagnostic parameters based on the GCC map (Fig 4A). The simplest was the overall average thickness (GCC-AVG). The difference between superior and inferior hemispheric averages (GCC-SID) was also computed.

To extract even more diagnostic information from the GCC map, we developed methods of analyzing the pattern of GCC loss. To do this, we computed maps of GCC loss as the fractional deviation (FD) map and the pattern deviation (PD) map. The FD map (Fig 4B) is the GCC map minus the normal reference map divided by the normal reference map. The pattern map is the GCC thickness map normalized (divided) by its own overall average. The PD map (Fig 4C) is the pattern map under consideration minus the normal reference pattern. The FD map shows the percentage of GCC loss. The PD map shows how the GCC pattern differs from normal.

Three pattern-based diagnostic parameters were then computed from the 2 derivative maps. The focal loss volume (FLV) is the sum FD in the region where there is significant focal loss. Significant focal loss is defined as PD >1.65 SD below the normal average (below the fifth percentile of normal distribution). Global loss volume (GLV) is the sum of FD in areas where FD is negative. Pattern coefficient of variation (PCV) is the root mean square of the PD map.

The image processing and diagnostic parameter calculations were programmed in MATLAB 7.0 (The MathWorks, Natick, MA).

Statistical Analyses

Both eyes of each participant were analyzed. The study sample was viewed as a clustered sample. The intereye correlation was

Figure 4. A perimetric glaucoma case example. All of the ganglion cell complex (GCC) parameters were abnormal (average = 71 μm; $P<0.5\%$; focal loss volume = 12.6%; $P<0.5\%$; global loss volume = 26.5%; $P<0.5\%$; pattern coefficient of variation = 21%; $P<0.5\%$; superior–inferior difference = 17.0 μm; $P<0.5\%$). **A**, The GCC map. **B**, Fractional deviation map with areas of significant focal loss marked by red hatching. **C**, GCC pattern deviation (PD) map. **D**, Disc photo showing inferotemporal rim loss. **E**, Visual field (VF) PD map. The VF was abnormal (pattern standard deviation = 16.5 dB; $P<0.5\%$); the glaucoma hemifield test was outside normal limits. The elliptical dashed line shows the area corresponding to the GCC maps. The superior VF defect corresponded with the inferior GCC loss and disc rim thinning.

accounted for in statistical tests by the use of a generalized estimating equation (GEE)[29] approach, linear mixed model,[30] or formulae derived for clustered samples.[31–33]

To compare the means, a generalized linear model[34] with a GEE approach was used to evaluate the mean difference between groups. The *P*-values for mean comparisons were based on a Wald test.[35] The model allows for non-Gaussian distributions in addition to Gaussian distributions for fitting the dependent variables. The normality of distribution was verified by inspection of histogram and a Kolmogorov–Smirnov test. We noticed that some participants had 1 eye in PPG and the other eye in PG groups. To avoid the off calculation in model parameter estimation, we compared PPG versus normal and PG versus normal, respectively. The tests were performed in a 1-tailed manner because we hypothesize that the means in the diseased groups are lower than in the normal group.

Intraclass correlation (ICC),[36] pooled SD,[37] and coefficients of variation (CV) were used to evaluate the reproducibility of diagnostic parameters. These indices were computed from linear mixed models in which the variance components for subject and eye variation were included to account for intrasubject correlation. To compare pooled SD or CV between diagnostic parameters, we generated the pooled SD or CV for each eye and used GEE paired *t*-tests for comparisons.

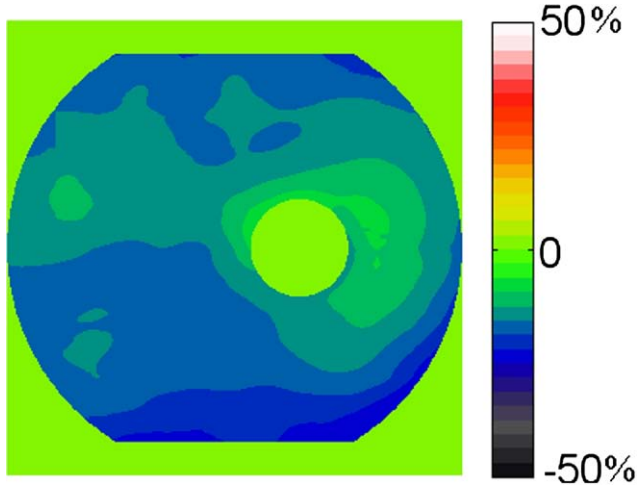

Figure 5. The average ganglion cell complex fractional deviation map of the perimetric glaucoma group.

Table 1. Characteristics of the Study Population

Group	Normal	Preperimetric Glaucoma	P*	Perimetric Glaucoma	P†
No. of participants‡	65	52	—	78	—
No. of eyes	125	76	—	109	—
Age (yrs)§	52.9±8.9	60.4±9.7	<0.0001	60.5±8.4	<0.0001
Female (% total)	68%	56%	0.2	56%	0.2
Race (% Caucasian)	88%	79%	0.2	73%	0.03
MD (dB)§	−0.1±1.0	−0.5±1.4	0.01	−4.6±4.4	<0.0001
PSD (dB)§	1.5±0.2	1.9±1.0	0.001	6.0±4.4	<0.0001
IOP (mmHg)§	14.7±2.5	16.4±3.3	0.004	15.2±3.5	0.3
CCT (μm)§	561.3±36.8	560.0±32.4	0.7	541.9±35.8	0.007

CCT = central corneal thickness; dB = decibels; IOP = intraocular pressure; MD = mean deviation (visual field); PSD = pattern standard deviation (visual field).
*P values for comparing normal and PPG groups.
†P values for comparing normal and PG groups.
‡Some participants have 1 eye diagnosed as PPG and the other eye diagnosed as PG.
§Mean value ± standard deviation.

Area under the receiver operating characteristic (AROC) curve was used to compare diagnostic power. To account for intereye correlation, the AROC was computed based on the formula of Obuchowski,[33] which extended the nonparametric method of DeLong et al[38] as applied to clustered data. The same method has been used in previous studies in ophthalmology[16,39] to handle intereye correlation.

To adjust for age imbalance between the normal, PG, and PPG groups, a logistic regression model with age and diagnostic parameter in covariates was used to generate the AROC. This method of compensating for age imbalance has been used in a previous ophthalmology study.[40] A GEE approach was added to the logistic regression model to account for the intereye correlation in the study sample.

For sensitivity and specificity, we computed thresholds for 5th and 1st percentiles. For a Gaussian distributed parameter, the percentiles can be formulated as $\text{mean}_N + Z_\alpha SD_N$, where mean_N and SD_N are the mean and SD of the normal group, $Z_\alpha = -1.65$ for the 5th percentile cutoff, and $Z_\alpha = -2.33$ for the first percentile cutoff. The parametric distribution of a non-Gaussian parameter was estimated based on 10 000 replicates, in which 1 eye was randomly selected from each participant. The SD_N and the standard error of sensitivity and specificity were computed based on the formulae for clustered data[31,32]; this method has been used in previous studies in ophthalmology.[16,39]

The AROC calculations were written in MATLAB 7.0 software and the other statistical calculations were performed with the SAS 9.1 software. The critical α level of statistical significance was set at 0.05.

Results

A total of 183 participants (328 eyes) with available RTVue GCC and Stratus scans were identified from the AIG central database. A total of 849 GCC scans were screened, 48 were excluded for low signal and 41 were excluded owing to segmentation error. The average SSI of the accepted GCC scans was 39.8. A total of 622 Stratus scans were screened; 12 scans were excluded owing to low SS. The average SS of the accepted Stratus scans was 8.3. Stratus scans that had segmentation error were rejected and retaken by the photographer so a failure rate was not available. Finally, 18 eyes were excluded owing to lack of valid FD-OCT or TD-OCT data. The remaining 310 eligible eyes from 178 participants were analyzed. The demographic and clinical information for each group were summarized in Table 1. Preperimetric glaucoma and PG participants were both significantly older than normal participants by approximately 7 years. The potential overestimation of AROC due to the age imbalance was removed using a logistic regression model as stated in Methods. There were more Caucasians in the normal group compared with the PG group. However, there was no significant difference between the racial groups in terms of the means of diagnostic parameters in the normal group. The PG group had central corneal thickness that were significantly thinner than the normal group, and the PPG group had significantly higher intraocular pressure than the normal group. Both PG and PPG groups had significantly worse VF parameters than the normal group. All participants had open angles by gonioscopy except 1 participant with narrow angles in the PPG group.

According Glaucoma Staging System 2 system, the 109 PG eyes were classified into stage 0 (18 eyes), borderline (14 eyes), stage 1 (20 eyes), stage 2 (17 eyes), stage 3 (20 eyes), stage 4 (16 eyes), and stage 5 (4 eyes). Forty-one eyes had localized defects, 24 eyes have mixed defects, and 12 eyes have generalized defects. Seventy-nine eyes (70.5%) had MD ≥−6.0 dB, 25 eyes (22.3%) had MD between −6.01 to −12.0 dB, and 8 eyes (7.1%) MD <−12 dB.

Table 2 summarizes the distribution statistics of each diagnostic parameter by group. All parameters were significantly worse in the PPG and PG groups compared with the normal group ($P<0.001$). Because SID, PCV, FLV, and GLV had nonnormal distributions (gamma distributions), these parameters were compared using the Wald test as described in Methods.

Repeatability was assessed by 3 measures: ICC, pooled SD, and CV of repeated measures (Table 3; available online at http://aaojournal.org) during the same session. The repeatability in the PPG and PG groups is important because it provides an indication of how well a parameter can track progression through stages of the disease. Because glaucoma primarily affects the GCC (inner 3 retinal layers), it should affect GCC thickness and MR thickness in parallel fashion, matching micrometer by micrometer. Thus, their relative precision in tracking glaucoma can be gauged by the pooled SD. The pooled SDs of FD-OCT GCC were significantly smaller than TD-OCT MR in the normal ($P = 0.005$) and PG ($P=0.02$) groups. The pooled SDs of FD-OCT MR were also significantly smaller than TD-OCT MR in the normal ($P=0.002$) and PG ($P=0.048$) groups. In PPG group, the P-values were close to statistical significance (0.08 for GCC and 0.07 for MR). We cannot assume that glaucoma would affect GCC and NFL the same

Table 2. The Distribution of Diagnostic Parameters by Group

Diagnostic Parameter	Normal		Preperimetric Glaucoma		Perimetric Glaucoma	
	Mean ± SD	*Range*	*Mean ± SD*	*Range*	*Mean ± SD*	*Range*
RTVue FD-OCT						
GCC-AVG (μm)	94.8±7.5	76.6–119.8	87.0±9.3	68.6–114.6	79.4±10.4	53.6–99.1
GCC-FLV (%)	−0.7±1.9	−17.0 to 0.0001	−2.3±2.7	−12.5 to 0.0001	−6.4±4.3	−14.5–0.0001
GCC-GLV (%)	−4.3±4.3	−21.1 to 0.001	−10.2±7.0	−26.6 to −0.1	−17.5±9.7	−42.1 to −1.0
GCC-PCV	0.076±0.036	0.041–0.360	0.090±0.034	0.051–0.240	0.133±0.046	0.051–0.227
GCC-SID (μm)	3.4±2.9	0.02–15.8	4.2±4.0	0.1–21.5	7.2±6.0	0.1–24.9
MR-AVG (μm)	228.5±13.2	203.1–261.6	218.9±12.1	194.9–252.3	212.1±12.4	180.9–237.0
Stratus TD-OCT						
NFL-AVG (μm)	98.9±8.3	79.5–131.4	87.7±13.1	60.2, 114.4	77.5±14.8	43.5, 127.5
MR-AVG (μm)	238.3±13.0	208.0–264.2	229.1±14.5	205.3–269.7	221.7±14.6	180.0–252.5

AVG = average; FD-OCT = Fourier-domain optical coherence tomography; FLV (%) = focal loss volume expressed as a percentage of the average GCC volume in the normal group; GCC = ganglion cell complex thickness; GLV = global loss volume; MR = macular retina thickness; NFL = nerve fiber layer thickness; PCV = pattern coefficient of variation; SD = standard deviation; SID = superior–inferior difference; TD-OCT = time-domain optical coherence tomography.

micrometer by micrometer, but their loss might be roughly proportional. Therefore, CV could provide an approximate comparison between the repeatability of GCC and NFL. The CVs of FD-OCT GCC were significantly smaller than TD-OCT NFL in the normal ($P = 0.0002$) and PG ($P<0.001$) groups, but not in the PPG group ($P = 0.11$). To compare the repeatability of all FD-OCT parameters, it is best to use the ICC because the pattern parameters (FLV, GLV, PCV, SID) have mean values close to zero (therefore, CVs are not meaningful) and have different units (therefore, SDs are not comparable). The FD-OCT GCC-AVG, GCC-GLV, and MR-AVG all have the highest ICC values of 0.99 in the PG and PPG groups and therefore may be the best parameters to watch for the tracking of glaucoma progression.

The AROC (Table 4) provided a summary measure of the accuracy of diagnosing glaucoma against the normal reference group. The MR average measured by FD-OCT and TD-OCT had equivalent AROC values. By isolating the inner retina, GCC-AVG significantly improved the diagnosis of PG (AROC = 0.90) compared with MR ($P = 0.021$). The pattern parameter GCC-GLV ($P = 0.01$) performed even better in diagnosing PG than GCC. The macular parameters GCC-AVG, GCC-FLV, and GCC-GLV had statistically equal ($P>0.1$) diagnostic power compared with NFL-AVG. For the diagnosis of PPG (versus normal), we found no significant difference between GCC parameters and MR. Diagnostic accuracy is also shown in the form of diagnostic sensitivities at 1st and 5th percentile cutoff thresholds (Table 5).

Table 4. Diagnostic Accuracy of Diagnostic Parameters

Diagnostic Parameter	Perimetric Glaucoma AROC (SE)	Preperimetric Glaucoma AROC (SE)
RTVue FD-OCT		
GCC-AVG (μm)	0.90 (0.02)	0.78 (0.05)
GCC-FLV (%)	0.92 (0.02)	0.73 (0.05)
GCC-GLV (%)	0.92 (0.02)	0.79 (0.04)
GCC-PCV	0.90 (0.02)	0.72 (0.05)
GCC-SID (μm)	0.80 (0.03)	*
MR-AVG (μm)	0.85 (0.03)	0.76 (0.05)
Stratus TD-OCT		
NFL-AVG (μm)	0.92 (0.02)	0.80 (0.05)
MR-AVG (μm)	0.85 (0.03)	0.76 (0.05)

AVG = average; AROC = area under the receiver operating curve; FD-OCT = Fourier-domain optical coherence tomography; FLV (%) = focal loss volume expressed as a percentage of the average GCC volume in the normal group; GCC = ganglion cell complex thickness; GLV = global loss volume; MR = macular retina thickness; NFL = nerve fiber layer thickness; PCV = pattern coefficient of variation; SE = standard error; SID = superior–inferior difference; TD-OCT = time-domain optical coherence tomography.
The accuracy of diagnosing PG and PPG against the reference normal group was assessed by the area under the receiver operating curve.
*The AROC was not significantly better than 0.5 and was omitted.

The odds ratio of having glaucoma for every 10 μm loss of tissue was 7.45 (95% confidence interval [CI], 4.14–13.40) for GCC-AVG, 5.06 (2.58, 9.92) for NFL and 2.69 (95% CI, 1.96–3.67), and 2.53 (95% CI, 1.84–3.47) for FD-OCT and TD-OCT MR, respectively. We note that, for each 10-μm of tissue loss, GCC predicts a significantly greater (3-fold) increase in the odds ratio than the loss of MR.

We chose a PG case with a very asymmetric VF to show how the locations of VF and disc rim defects correlated with GCC loss (Fig 4). The predominantly inferior GCC loss correlated with the inferior disc rim loss and superior VF defect.

The pattern of GCC loss averaged over the PG group (Fig 5) showed sparing of the maculopapillar bundle, which was tilted in accordance with the fact that the fovea is below the level of the disc. The severest fractional loss occurred at the superior and inferior edges of the map, corresponding with the locations of the superior and inferior arcuate NFL bundles.

We chose a PPG case (Fig 6; available online at http://aaojournal.org) where the average GCC was within normal and the pattern parameters were abnormal to investigate how such a situation could arise. In this case, the GCC loss was localized primarily to an area above the fovea, and the abnormality was easily picked up by the pattern-based parameters. But the GCC was actually thicker than average in the maculopapillar area, which contributed toward an average GCC thickness that was still within the normal range. The focal loss of GCC in the superior macula was as much as 30%, corresponding to a mild thinning of the superotemporal disc rim, whereas the VF was essentially normal.

To investigate whether GCC can help to detect glaucomatous abnormalities not picked up by NFL, we constructed Venn diagrams of GCC and NFL abnormalities in both the PG and PPG groups (Fig 7). We combined the 3 best GCC parameters—GCC abnormality was defined as GCC-AVG, FLV, or GLV below the percentile of the normal reference. Abnormal NFL was defined by

Table 5. Sensitivity and Specificity of Diagnostic Parameters

Threshold Parameter	5th Percentile			1st Percentile		
	Sensitivity (PG)	*Sensitivity (PPG)*	*Specificity*	*Sensitivity (PG)*	*Sensitivity (PPG)*	*Specificity*
RTVue FD-OCT						
GCC-AVG	0.61 (0.05)	0.34 (0.06)	0.95 (0.02)	0.43 (0.05)	0.13 (0.04)	0.99 (0.01)
GCC-FLV	0.72 (0.05)	0.30 (0.05)	0.95 (0.02)	0.36 (0.05)	0.04 (0.03)	0.99 (0.01)
GCC-GLV	0.63 (0.06)	0.33 (0.06)	0.95 (0.02)	0.46 (0.05)	0.11 (0.03)	0.98 (0.01)
GCC-PCV	0.6 (0.05)	0.17 (0.05)	0.97 (0.02)	0.41 (0.05)	0.05 (0.03)	0.98 (0.01)
GCC-SID	0.28 (0.04)	0.09 (0.04)	0.94 (0.02)	0.16 (0.04)	0.04 (0.02)	0.99 (0.01)
MR-AVG	0.36 (0.05)	0.2 (0.06)	0.97 (0.02)	0.14 (0.04)	0.01 (0.01)	1 (0)
Stratus TD-OCT						
NFL-AVG	0.75 (0.04)	0.39 (0.06)	0.97 (0.02)	0.6 (0.05)	0.3 (0.06)	0.98 (0.02)
MR-AVG	0.37 (0.05)	0.26 (0.06)	0.97 (0.02)	0.21 (0.05)	0.05 (0.03)	0.99 (0.01)

AVG = average; FD-OCT = Fourier-domain optical coherence tomography; FLV (%) = focal loss volume expressed as a percentage of the average GCC volume in the normal group; GCC = ganglion cell complex thickness; GLV = global loss volume; MR = macular retina thickness; NFL = nerve fiber layer thickness; PCV = pattern coefficient of variation; PG = perimetric glaucoma group; PPG = preperimetric glaucoma group; SID = superior–inferior difference; TD-OCT = time-domain optical coherence tomography.

NFL-AVG below the 5th percentile; GCC detected an additional 9% of PG cases and 11% of PPG cases that were not detected by NFL.

Discussion

Although glaucoma is clinically defined as optic disc cupping with corresponding VF defects, the underlying disease process in glaucoma is the loss of RGC.[1–3] Approximately one third of the RGC population resides within the posterior pole. In the macula, the RGC layer is >1 cell layer thick with an RGC body diameter 10 to 20 times larger compared with their axons. In addition, the central retina has less variability in cell density compared with peripheral retina.[41] Thus, detecting RGC loss in the macula may allow earlier detection of glaucoma in some cases.

Ishikawa et al[15] developed a software algorithm to perform automatic retinal layer segmentation in the macula for the commercially available Stratus TD-OCT and reported that macular inner retinal layer thickness measurements could indeed be used to discriminate normal from glaucomatous eyes. They found that the outer retinal layers were not affected in glaucoma. However, one of the limitations of the study was variable scan quality. More than one third of their scans on glaucomatous eyes had to be excluded from segmentation analysis owing to poor quality scans related to speckle noise and uneven tissue reflectivity. The authors suggested that higher resolution and improved signal quality (higher signal-to-noise ratio), as provided by FD-OCT, may be needed for better quality image acquisition to allow accurate retinal layer segmentation.

Leung et al[42] used the Stratus TD-OCT to evaluate macular NFL thinning in glaucoma using the 3.4-mm diameter circular scan pattern (fast RNFL scan). They reported a reduction in macular NFL thickness in glaucomatous eyes compared with normal eyes. However, they found that measurement of macular NFL thickness offered no advantage over measurement of total macular thickness for glaucoma detection. In their study, circumpapillary NFL thickness outperformed macular NFL and total macular thickness in the ability to detect glaucoma and correlate with visual function.

Greenfield et al[43] reported that OCT-derived macular thickness was well correlated with changes in visual function and RNFL structure in moderately advanced glaucoma. They reported a strong correlation between mean macular thickness and VF MD ($r^2 = 0.47$; $P<0.001$), and suggested that reduced macular thickness could be a surrogate for loss of RGCs in glaucoma.

Our study confirmed that MR thickness by either FD-OCT or Stratus TD-OCT was a less accurate parameter for glaucoma detection than Stratus NFL thickness. Other investigators, including Wollstein et al,[13] Guedes et al,[44] and Medeiros et al[45] have also reported higher AROC values for Stratus NFL compared with Stratus MR for glaucoma detection. Our AROC values for MR by TD-OCT (AROC 0.85) and FD-OCT (AROC 0.85) were slightly higher than values previously reported by Medeiros et al (AROC 0.75–0.81).[45]

In the current study, we report on the development of novel diagnostic parameters using FD-OCT to look for glaucoma in the macula. The faster speed of FD-OCT (65× Stratus TD-OCT) allows high-density scanning over a large region of the macula with less motion artifact. The resolu-

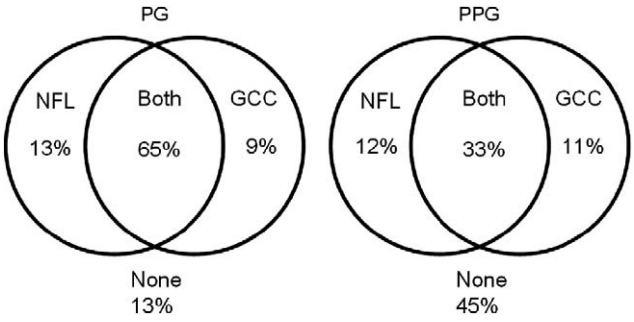

Figure 7. Venn diagrams showing the overlap between abnormal nerve fiber layer (NFL) and ganglion cell complex (GCC) thicknesses in both perimetric glaucoma (PG) and preperimetric glaucoma (PPG) groups. Abnormalities were detected at the 5 percentile level.

tion of the RTVue FD-OCT device is also 2 times better than Stratus TD-OCT. The combination of higher definition (denser sampling) and higher resolution significantly improved the precision (repeatability) of both MR and GCC measurement, which could improve the ability to track glaucomatous thinning over time.

Our study also showed that the GCC average measured by the RTVue FD-OCT were significantly better at diagnosing glaucoma in the PG group, compared with the MR average measured by either FD-OCT or TD-OCT. Thus, isolating GCC from the outer retina improved the diagnostic power of the macular measurement. This could be explained by the fact that the outer retina, which is not much affected by glaucoma, takes up 65% to 70% of total retinal thickness and, therefore, could contribute variation in thickness that decreases discriminant power. The diagnostic power of GCC average was also higher than that of MR in the discrimination between PPG and normal eyes, but the advantage was not statistically significant. This could be explained by the smaller PPG group size. Also, the PPG group is primarily defined by detection of rim notching on disc photographs, which may bias the diagnosis toward those with rim loss primarily in the superior and inferior poles of the optic nerve head, while missing those with rim thinning more temporally. So the PPG group may have a lower percentage of cases with significant macular ganglion cell loss. Macular GCC measurement by OCT may detect PPG earlier in those cases where the ganglion cell loss is more predominantly macular rather than peripheral. We will study this possibility in a group of ocular hypertensives and other glaucoma suspects enrolled in the AIGS.

Our study showed that FD-OCT macula GCC parameters did not have higher AROC than TD-OCT circumpapillary NFL; they were statistically equal. This is understandable; the circumpapillary NFL samples nearly all axons arising from ganglion cells, whereas the GCC scan only covers the macular area. However, the GCC scan samples the macula better and may be able to better detect glaucoma cases where macular loss occurs early. Thus, GCC and NFL parameters may be complementary. In our preliminary investigation with the Venn diagram (Fig 7), the addition of GCC data to NFL increased detection rate from 78% to 87% in the PG group and from 45% to 56% in the PPG group. We will further study whether a composite parameter incorporating both FD-OCT NFL and GCC parameters could significantly increase diagnostic accuracy. The combination of diagnostic parameters from different anatomic areas have been found to boost diagnostic accuracy in previous studies.[39,46]

Wider and finer sampling of the macular regions in <1 second was made possible by the higher speed of FD-OCT. This facilitated the analysis of patterns of GCC loss. We designed several pattern-based parameters that looked at different aspects of the GCC loss pattern and have the potential to be used in a complementary fashion. The SID parameter was designed to detect cases where GCC loss is asymmetric between superior and inferior macular regions. The GLV and FLV parameters sum up the volume of GCC loss in the macula with differing levels of focality. The FLV parameter is more focal because it only sums loss in regions where the GCC is thin in both absolute (GCC <normal) and relative (PD <5th percentile) terms. The PCV parameter is purely based on the PD map and detects any change in the GCC pattern. We found that FLV and GLV had higher diagnostic accuracy than the simple average for the diagnosis of PG. This must mean that, in some cases, pattern parameters are more sensitive or more specific. For example, pattern parameters could be more sensitive in eyes that have started with an above average GCC thickness and where GCC loss is focal rather than diffuse (example shown in Fig 6; available online at http://aaojournal.org). Pattern parameters could be more specific in a normal eye that had at baseline a thinner GCC with a normal distribution pattern.

An advantage of the GCC map is that it could be correlated with VF defects point by point. When they correspond, one may be more confident that the defects are real rather than artifacts. An example of this correspondence was shown in Figure 4. Each millimeter on the retina corresponds to about 3.5° on the VF. Therefore the GCC map (7×6 mm) subtends about 11° superiorly and inferiorly, 10° nasally, and 15° temporally. It covers about half of the area of the standard Humphrey 24-2 VF (Fig 4E), and is up/down reversed relative to the VF owing to optical projection in the eye. The example in Figure 4 showed that in the case of end-stage VF defect (−35 dB), the fractional GCC loss was approximately 50%. Possibly residual glial tissue maintains 50% thickness, even when nearly all ganglions cells were lost.

One of the limitations of the study is that the normal group was used to both define the normal reference GCC pattern and assess diagnostic specificity. This could theoretically cause a false inflation of the specificity and AROC values of the GCC pattern parameters. However, we believe this effect was probably very small because there is no reason why the GCC distribution pattern would vary between normal populations, and we had a sufficient number of normal participants to obtain a smooth normal reference GCC map (Fig 3F; available online at http://aaojournal.org) with a tight standard error of 0.9 μm. Nevertheless, a separate study with an independent population is needed to confirm our conclusions. The GCC segmentation and the pattern parameters described herein have been licensed to Optovue, Inc. The GCC map and average was released in RTVue software version 3.0 and the pattern parameters were released in version 4.0. We invite other investigators to use the commercially released software to validate our findings.

In summary, we found that GCC measurements with FD-OCT have better diagnostic accuracy and repeatability compared with MR measurements by either TD-OCT or FD-OCT. Analysis of GCC loss pattern further boosted diagnostic accuracy. Independent investigations are needed to validate the findings of this pilot study.

References

1. Quigley HA, Dunkelberger GR, Green WR. Retinal ganglion cell atrophy correlated with automated perimetry in human eyes with glaucoma. Am J Ophthalmol 1989;107:453–64.
2. Quigley HA, Miller NR, George T. Clinical evaluation of nerve fiber layer atrophy as an indicator of glaucomatous optic nerve damage. Arch Ophthalmol 1980;98:1564–71.

3. Sommer A, Miller NR, Pollack I, et al. The nerve fiber layer in the diagnosis of glaucoma. Arch Ophthalmol 1977;95:2149–56.
4. Sommer A, Quigley HA, Robin AL, et al. Evaluation of nerve fiber layer assessment. Arch Ophthalmol 1984;102:1766–71.
5. Pederson JE, Anderson DR. The mode of progressive disc cupping in ocular hypertension and glaucoma. Arch Ophthalmol 1980;98:490–5.
6. Sommer A, Katz J, Quigley HA, et al. Clinically detectable nerve fiber atrophy precedes the onset of glaucomatous field loss. Arch Ophthalmol 1991;109:77–83.
7. Quigley HA, Katz J, Derick RJ, et al. An evaluation of optic disc and nerve fiber layer examinations in monitoring progression of early glaucoma damage. Ophthalmology 1992; 99:19–28.
8. Airaksinen PJ, Drance SM, Douglas GR, et al. Diffuse and localized nerve fiber loss in glaucoma. Am J Ophthalmol 1984;98:566–71.
9. Harwerth RS, Carter-Dawson L, Shen F, et al. Ganglion cell losses underlying visual field defects from experimental glaucoma. Invest Ophthalmol Vis Sci 1999;40:2242–50.
10. Zeimer R, Asrani S, Zou S, et al. Quantitative detection of glaucomatous damage at the posterior pole by retinal thickness mapping: a pilot study. Ophthalmology 1998;105:224–31.
11. Huang D, Swanson EA, Lin CP, et al. Optical coherence tomography. Science 1991;254:1178–81.
12. Bagga H, Greenfield DS, Knighton RW. Macular symmetry testing for glaucoma detection. J Glaucoma 2005;14:358–63.
13. Wollstein G, Schuman JS, Price LL, et al. Optical coherence tomography (OCT) macular and peripapillary retinal nerve fiber layer measurements and automated visual fields. Am J Ophthalmol 2004;138:218–25.
14. Lederer DE, Schuman JS, Hertzmark E, et al. Analysis of macular volume in normal and glaucomatous eyes using optical coherence tomography. Am J Ophthalmol 2003;135: 838–43.
15. Ishikawa H, Stein DM, Wollstein G, et al. Macular segmentation with optical coherence tomography. Invest Ophthalmol Vis Sci 2005;46:2012–7.
16. Tan O, Li G, Lu AT, et al. Mapping of macular substructures with optical coherence tomography for glaucoma diagnosis. Ophthalmology 2008;115:949–56.
17. Wojtkowski M, Srinivasan V, Fujimoto JG, et al. Three-dimensional retinal imaging with high-speed ultrahigh-resolution optical coherence tomography. Ophthalmology 2005;112:1734–46.
18. Leitgeb R, Hitzenberger CK, Fercher AF. Performance of Fourier domain vs. time domain optical coherence tomography. Opt Express [serial online] 2003;11:889–94. Available at: http://www.opticsinfobase.org/oe/abstract.cfm?uri=oe-11-8-889. Accessed May 3, 2009.
19. Choma MA, Sarunic MV, Yang C, Izatt JA. Sensitivity advantage of swept-source and Fourier domain optical coherence tomography. Opt Express [serial online] 2003;11:2183–9. Available at: http://www.opticsinfobase.org/oe/abstract.cfm?uri=oe-11-18-2183. Accessed May 3, 2009.
20. Wojtkowski M, Leitgeb R, Kowalczyk A, et al. In vivo human retinal imaging by Fourier domain optical coherence tomography. J Biomed Opt 2002;7:457–63.
21. Wojtkowski M, Kowalczyk A, Leitgeb R, Fercher AF. Full range complex spectral optical coherence tomography technique in eye imaging. Opt Lett 2002;27:1415–7.
22. de Boer JF, Cense B, Park BH, et al. Improved signal-to-noise ratio in spectral-domain compared with time-domain optical coherence tomography. Opt Lett 2003;28:2067–9.
23. Wojtkowski M, Bajraszewski T, Targowski P, Kowalczyk A. Real-time in vivo imaging by high-speed spectral optical coherence tomography. Opt Lett 2003;28:1745–7.
24. Yun SH, Tearney GJ, Bouma BE, et al. High-speed spectral-domain optical coherence tomography at 1.3 mum wavelength. Opt Express [serial online] 2003;11:3598–604. Available at: http://www.opticsinfobase.org/oe/abstract.cfm?uri=oe-11-26-3598. Accessed May 3, 2009.
25. Nassif N, Cense B, Park BH, et al. In vivo human retinal imaging by ultrahigh-speed spectral domain optical coherence tomography. Opt Lett 2004;29:480–2.
26. Nassif NA, Cense B, Park BH, et al. In vivo high-resolution video-rate spectral-domain optical coherence tomography of the human retina and optic nerve. Opt Express [serial online] 2004;12:367–76. Available at: http://www.opticsinfobase.org/oe/abstract.cfm?uri=oe-12-3-367. Accessed May 3, 2009.
27. Chen TC, Cense B, Pierce MC, et al. Spectral domain optical coherence tomography: ultra-high speed, ultra-high resolution ophthalmic imaging. Arch Ophthalmol 2005;123:1715–20.
28. Brusini P, Filacorda S. Enhanced Glaucoma Staging System (GSS 2) for classifying functional damage in glaucoma. J Glaucoma 2006;15:40–6.
29. Liang KY, Zeger SL. Longitudinal data analysis using generalized linear models. Biometrika 1986;73:13–22.
30. Laird NM, Ware JH. Random-effects models for longitudinal data. Biometrics 1982;38:963–74.
31. Williams RL. A note on robust variance estimation for cluster-correlated data. Biometrics 2000;56:645–6.
32. Rao JN, Scott AJ. A simple method for the analysis of clustered binary data. Biometrics 1992;48:577–85.
33. Obuchowski NA. Nonparametric analysis of clustered ROC curve data. Biometrics 1997;53:567–78.
34. McCullagh P, Nelder J. Generalized Linear Models. 2nd ed. London: Chapman and Hall; 1989:21–44. Monographs on Statistics and Applied Probability. vol. 37.
35. Snijders T, Bosker R. Multilevel Analysis: An Introduction to Basic and Advanced Multilevel Modeling. London: Sage; 1999:86.
36. Cinelli RA, Tozzini V, Pellegrini V, et al. Coherent dynamics of photoexcited green fluorescent proteins. Phys Rev Lett 2001;86:3439–42.
37. Warmke J, Drysdale R, Ganetzky B. A distinct potassium channel polypeptide encoded by the *Drosophila eag* locus. Science 1991;252:1560–2.
38. DeLong ER, DeLong DM, Clarke-Pearson DL. Comparing the areas under two or more correlated receiver operating characteristic curves: a nonparametric approach. Biometrics 1988;44:837–45.
39. Lu AT, Wang M, Varma R, et al, Advanced Imaging for Glaucoma Study Group. Combining nerve fiber layer parameters to optimize glaucoma diagnosis with optical coherence tomography. Ophthalmology 2008;115:1352–7.
40. Deleon-Ortega JE, Arthur SN, McGwin G Jr, et al. Discrimination between glaucomatous and nonglaucomatous eyes using quantitative imaging devices and subjective optic nerve head assessment. Invest Ophthalmol Vis Sci 2006;47:3374–80.
41. Glovinsky Y, Quigley H, Pease ME. Foveal ganglion cell loss is size dependent in experimental glaucoma. Invest Ophthalmol Vis Sci 1993;34:395–400.
42. Leung CK, Chan WM, Yung WH, et al. Comparison of macular and peripapillary measurements for the detection of glaucoma: an optical coherence tomography study. Ophthalmology 2005;112:391–400.
43. Greenfield DS, Bagga H, Knighton RW. Macular thickness changes in glaucomatous optic neuropathy detected using optical coherence tomography. Arch Ophthalmol 2003;121:41–6.

44. Guedes V, Schuman JS, Hertzmark E, et al. Optical coherence tomography measurement of macular and nerve fiber layer thickness in normal and glaucomatous human eyes. Ophthalmology 2003;110:177–89.
45. Medeiros FA, Zangwill LM, Bowd C, et al. Evaluation of retinal nerve fiber layer, optic nerve head, and macular thickness measurements for glaucoma detection using optical coherence tomography. Am J Ophthalmol 2005;139:44–55.
46. Zangwill LM, Chan K, Bowd C, et al. Heidelberg retina tomograph measurements of the optic disc and parapapillary retina for detecting glaucoma analyzed by machine learning classifiers. Invest Ophthalmol Vis Sci 2004;45:3144–51.

Footnotes and Financial Disclosures

Originally received: July 7, 2008.
Final revision: May 12, 2009.
Accepted: May 13, 2009.
Available online: September 10, 2009. Manuscript no. 2008-820.

[1] Doheny Eye Institute and Department of Ophthalmology, Keck School of Medicine, University of Southern California, Los Angeles, California.

[2] Department of Ophthalmology, University of Pittsburgh School of Medicine, Pittsburgh, Pennsylvania.

Financial Disclosure(s):
David Huang - Patent royalty, stock options, travel support, and grant support - Optovue, Inc.; Patent royalty - Zeiss Meditec, Inc.

Joel S. Schuman – Lecturer - Optovue, Inc.; Patent royalty, travel support, and grant - Carl Zeiss Meditec, Inc.

Ou Tan - Patent royalty, grant support - Optovue, Inc.

Vikas Chopra - Travel support - Optovue, Inc.

Supported by NIH grants R01 EY013516 and P30 EY03040, a grant from Research to Prevent Blindness, and a grant from Optovue, Inc.

Vikas Chopra and Ake Lu made equal contributions to the manuscript.

Correspondence:
Ou Tan, PhD, Doheny Eye Institute, DVRC160-C, 1355 San Pablo Street, Los Angeles, CA 90033. E-mail: otan@usc.edu.

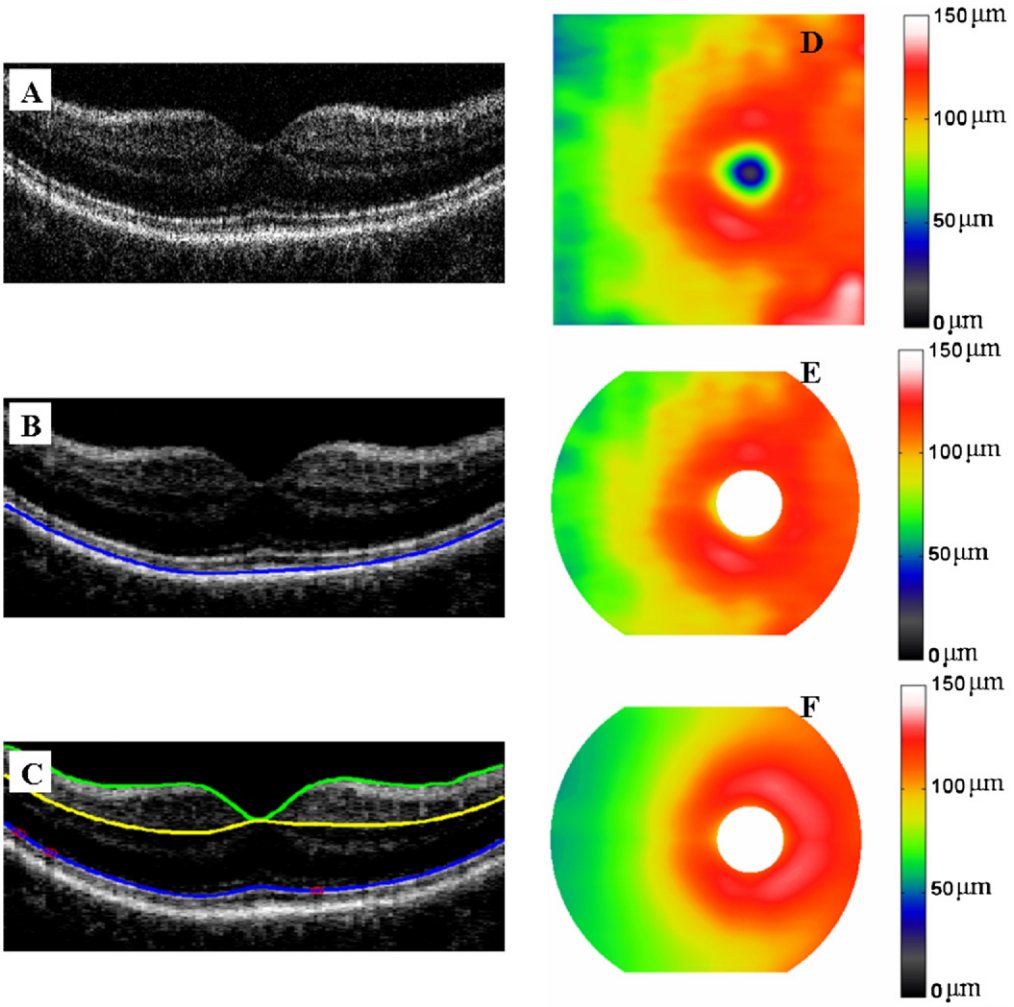

Figure 3. Image processing steps in the automated measurement of ganglion cell complex (GCC) and retinal thickness. **A**, Vertical optical coherence tomography (OCT) cross-section from the GCC scan is shown. **B**, The OCT image was low-pass filtered and resampled at lower definition to suppress speckle and speed processing. The photoreceptor pigment epithelium complex (PPC, blue line) was identified. **C**, The inner segment/outer segment junction (blue line) was detected from within the PPC. The inner limited membrane (ILM; green line) and outer boundary of the outer plexiform layer (yellow line) were also detected. Blood vessel shadowed axial-scans (a-scans; red circle) were replaced with adjacent a-scans to avoid interruption of boundary lines. **D**, Macular GCC thickness map was obtained by interpolation of the GCC profiles from the 16 OCT cross-sections in the GCC scan pattern. **E**, The GCC map was recentered on the foveal depression. Unreliable portions of the map were removed (cropped out on map shown). These include the foveal area (1.5 mm diameter), top and bottom 0.5 mm, and the corner regions with distance from map center >3.5 mm. **F**, The reference GCC map is averaged from all eyes in the normal group.

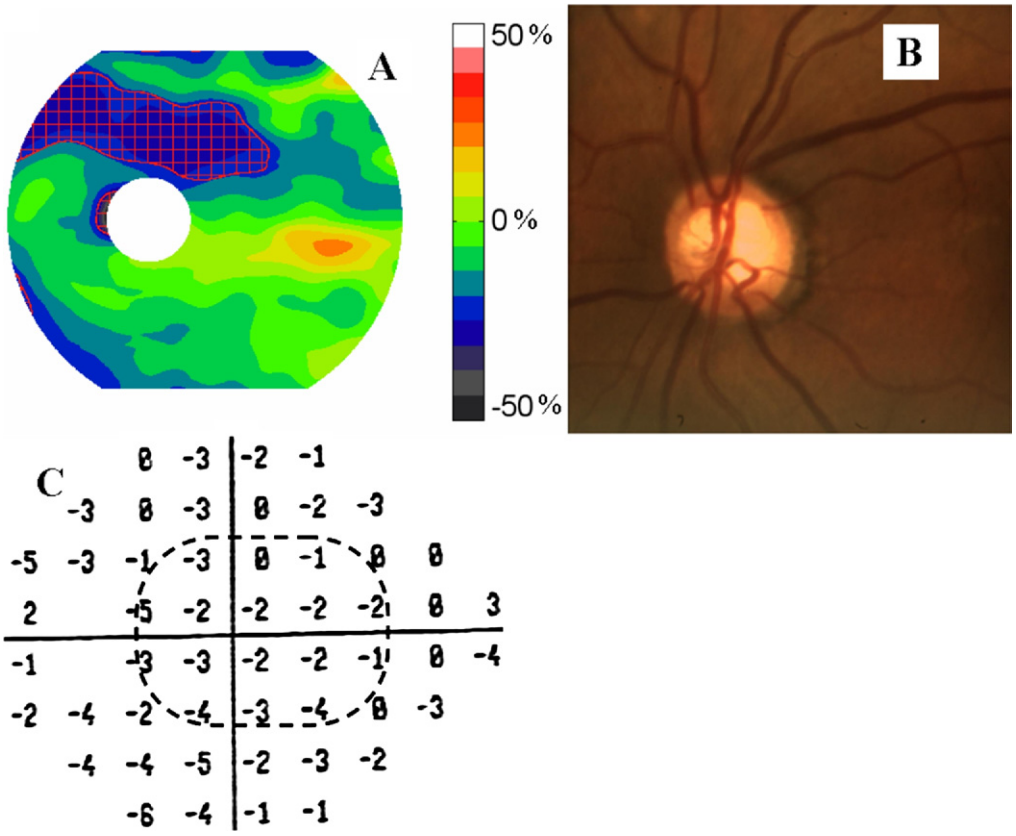

Figure 6. A preperimetric glaucoma case example. **A**, Ganglion cell complex (GCC) fraction deviation map. Some of the GCC parameters were abnormal (average = 82.5 μm; $P>5\%$; focal loss volume = 4.9%; $P<0.5\%$; global loss volume = 13.2%; $P<0.5\%$; pattern coefficient of variation = 13%; $P>5\%$; superior–inferior difference = −12.1 μm; $P<0.5\%$). **B**, Disc photograph showed mild thinning of the superotemporal rim. **C**, Visual field pattern deviation map showed scattered shallow depressions that were within the range of normal variation.

Table 3. Repeatability of Diagnostic Parameters

	Normal			Preperimetric Glaucoma			Perimetric Glaucoma		
Diagnostic Parameters	*ICC*	*SD*	*CV*	*ICC*	*SD*	*CV*	*ICC*	*SD*	*CV*
RTVue FD-OCT									
GCC-AVG (μm)	0.98	1.03	1.09	0.99	1.06	1.23	0.99	0.98	1.25
GCC-FLV (%)	0.91	0.38		0.96	0.59		0.95	1.01	
GCC-GLV (%)	0.98	0.68		0.99	0.90		0.99	1.01	
GCC-PCV	0.85	0.01		0.92	0.01		0.93	0.01	
GCC-SID (μm)	0.94	1.12		0.95	1.24		0.97	1.61	
MR-AVG (μm)	0.99	1.20	0.52	0.99	1.06	0.49	0.99	1.36	0.65
Stratus TD-OCT									
NFL-AVG (μm)	0.96	1.71	1.72	0.99	1.52	1.75	0.98	2.22	2.86
MR-AVG (μm)	0.97	2.17	0.91	0.93	3.69	1.61	0.96	3.01	1.36

AVG = average; CV = coefficient of variation; FD-OCT = Fourier-domain optical coherence tomography; FLV (%) = focal loss volume expressed as a percentage of the average GCC volume in the normal group; GCC = ganglion cell complex thickness; GLV = global loss volume; ICC = intraclass correlation; MR = macular retina thickness; NFL = nerve fiber layer thickness; PCV = pattern coefficient of variation; SD = pooled standard deviation; SID = superior–inferior difference; TD-OCT = time-domain optical coherence tomography.